Int. J. Electron. Commun. (AEÜ) 187 (2024) 155546

Contents lists available at ScienceDirect

Int. J. Electron. Commun. (AEÜ)

journal homepage: www.elsevier.com/locate/aeue

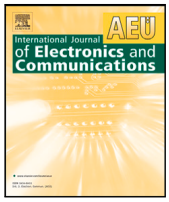

Error rates of optically pre-amplified PPM wireless systems with coding and arbitrary optical filter response

Konstantinos Yiannopoulos *, Nikos C. Sagias, Ioannis Moscholios

Department of Informatics and Telecommunications, University of the Peloponnese, Akadimaikou G.K. Vlachou, Tripoli, 22131, Arcadia, Greece

ARTICLE INFO

Keywords:
Optical wireless communications
Pulse position modulation
Optical filter
Optical amplifier
Karhunen–Loeve expansion
Bit error probability
LDPC error correction

ABSTRACT

We present novel results for the uncoded and coded bit-error probability (BEP) of optically pre-amplified pulse-position modulation (PPM) wireless systems. For uncoded systems, a novel analytic method for the evaluation of the BEP is derived. The method takes into account the non-ideal optical filter response and utilizes a finite Karhunen–Loève series expansion to calculate the BEP. Using the proposed approach, it is possible to accurately evaluate the PPM BEP for arbitrarily shaped filters where the well-established χ^2 method only provides approximate results. Considering a Lorentzian filter response, the discrepancy between the two methods amounts to 0.5 dB in a variety of filter bandwidths and PPM modulation orders. The Lorentzian filter response was chosen as an illustrative practical example whose series can be calculated analytically. The proposed method is also valid for any type of optical filter for which the Karhunen–Loève series expansion can be calculated analytically or numerically. Due to the finite number of terms that are required irrespective of the signal energy level, the proposed method can also be applied without loss of accuracy to assess the system performance under the effects of turbulence and adverse weather conditions. For coded systems with Lorentzian filters, Monte-Carlo simulations are utilized to evaluate the BEP performance of the 5G LDPC codes, and it is demonstrated that they impart an energy gain up to 3.3 dB for 4–PPM and 2.3 dB for 16–PPM at a target BEP of 10^{-5}. The optimal code rates are also discussed for several combinations of the optical filter bandwidth and PPM modulation order and it is shown that in almost all of the cases the optimal code rate is 11/13. Moreover, the sum-product and min-sum decoders perform within 0.1 dB from each other for the best code rates, which points towards the utilization of the min-sum decoder in all settings, since its operation does not require knowledge of the filter parameters. Finally, the comparison between the coded systems with Lorentzian and ideal passband filters exhibits the same 0.5 dB discrepancy that was observed for uncoded systems.

1. Introduction

Optical amplification and PPM have found applications in challenging optical wireless communication environments [1–12], such as atmospheric and space communications, since the losses that are introduced by the transmission of optical beams in long distances call for highly sensitive receivers [13–16]. The accurate modeling of optically pre-amplified receivers has attracted attention and initial efforts considered ideal passband optical filters [17], leading to the statistical description of the signal and noise via the χ^2 distribution. The χ^2 distribution has been extensively utilized to assess the performance in receivers with wide optical filters [15,18,19], although it proves less accurate in systems where the filter response deviates from the ideal passband one [20].

To our knowledge, the BEP performance of pre-amplified PPM receivers has not been previously evaluated for optical filters with arbitrary response. In this work, we perform this study for both the uncoded and coded systems. With respect to the uncoded systems, we derive a novel analytical method for the BEP evaluation. The method uses a Karhunen–Loève (K–L) expansion of the filtered signal and noise, which provides a highly accurate representation via a truncated sum with a minimum number of terms [21]. The K-L expansion also decorrelates the noise components and each term of the sum becomes a random variable that is independent from the rest. This enables the calculation of the Laplace transform of the total signal as a product of the individual transforms of the respective random variables. Even though the exact distribution that corresponds to the resulting Laplace transform is not known, since it deviates from the χ^2 one, we demonstrate that the PPM

* Corresponding author.
E-mail address: kyianno@uop.gr (K. Yiannopoulos).

https://doi.org/10.1016/j.aeue.2024.155546
Received 1 June 2024; Accepted 29 September 2024
Available online 5 October 2024

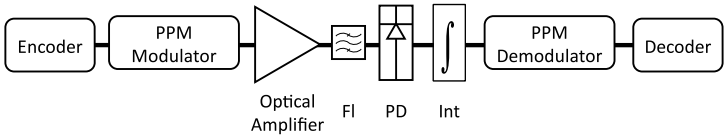

Fig. 1. Setup for the optically pre-amplified PPM communication system. Fl: optical filter, PD: photodiode, Int: integrator.

BEP can be calculated from the Laplace transform only, and we provide exact analytical relations for binary PPM and accurate approximations for higher modulation orders. Compared to the χ^2 statistics, our method is more accurate since it makes no assumptions, such as identical noise variances over the whole optical spectrum. The results show that the χ^2 approximation is inaccurate up to approximately 0.5 dB for Lorentzian response filters, irrespective of the filter bandwidth and the modulation order. For an ideal passband filter, the proposed method produces results that are in perfect agreement with the χ^2 approximation [19]. Even though the presented results correspond to filters with analytically available K-L expansions, the method is also applicable in scenarios where the filter expansion can be calculated numerically.

Regarding the coded systems, we consider the LDPC codes of the 5G standard [22], since we have recently demonstrated their error-correction capabilities in pre-amplified PPM receivers with ideal passband filters [23]. A key differentiation of this current work stems from the inability to analytically derive the received signal statistics, which makes the calculation of the likelihood function impossible. The likelihood function is required to calculate the PPM symbol probabilities [24], and subsequently, the received bit likelihoods [23] that constitute the inputs to the LDPC decoders for error-correction. In order to bypass this difficulty, we approximate the unknown function and assess the BEP performance of the sum–product and min-sum decoders via simulations. The results show that a significant gain can be expected in comparison with the uncoded systems, while both decoders exhibit a similar performance irrespective of the optical filter width and the modulation order. It is also shown that the best performance is expected for code rates between 2/3 and 11/13.

The rest of the paper is organized as follows: Section 2 describes the receiver model of the uncoded system and presents novel analytic formulas for the BEP evaluation. The section also reports the results that have been obtained using the analytic relations for the two optical filter types. Section 3 briefly describes the structure of the 5G LDPC codes and the implementation of the min-sum and sum–product decoders. It then details the proposed approximations of the bit likelihoods, which are required to perform the Monte-Carlo simulations and assess the BEP performance of the coded system. Finally, Section 4 summarizes the main findings of this work and concludes the paper.

2. Uncoded BEP evaluation

We consider an optically pre-amplified receiver that is shown in Fig. 1. The optical signal is amplified and filtered in the optical domain, and a polarizer is employed to discard the orthogonally polarized noise component. A photodiode converts the optical signal and the electrical signal is integrated over the duration of each PPM slot. The PPM demodulator monitors the recorded energy at each slot and decides upon the received symbol based on the maximum received energy (soft decision decoding).

2.1. Receiver model

We utilize a K-L expansion to express the filtered noise as [17]

$$n(t) = \sum_{k=1}^{\infty} n_k\, \phi_k(t) = \sum_{k=1}^{\infty} \left(n'_k + i\, n''_k\right)\, \phi_k(t), \qquad |t| \le \frac{T_s}{2}, \tag{1}$$

where T_s is the PPM slot duration. n'_k and n''_k are the real and imaginary noise components, respectively, and are assumed to be independent zero-mean Gaussian random variables (RVs). The eigenfunctions $\phi_k(t)$ form an orthonormal basis over the time interval $\left[-T_s/2,\, T_s/2\right]$ and are calculated from the integral equation

$$\int_{-\frac{T_s}{2}}^{\frac{T_s}{2}} R_n(y-x)\, \phi_k(x)\, dx = \lambda_k\, \phi_k(y), \tag{2}$$

where $R_n(\tau)$ is the autocorrelation function of the optical filter. The appearing eigenvalues λ_k determine the variances of the noise components n_k which are given by $\lambda_k\, N_0$, assuming that the noise spectral density at the output of the amplifier $N_0 = n_{sp}\, h\, f\, (G-1)$ remains constant over the filter response. The optical signal at the filter output may also be expanded over the basis that is formed by $\phi_k(t)$ following

$$s(t) = \sqrt{E_s} \sum_{k=1}^{\infty} s_k\, \phi_k(t), \qquad |t| \le \frac{T_s}{2}, \tag{3}$$

where E_s is the signal energy within the PPM slot and relates to the average energy per bit as $E_s = E_b \log_2(Q)$, with Q denoting the modulation order. The appearing expansion terms s_k are calculated either in the time or the frequency domain following

$$\begin{aligned} s_k &= \frac{1}{\sqrt{E_s}} \int_{-\frac{T_s}{2}}^{\frac{T_s}{2}} s(t)\, \phi_k(t)\, dt \\ &= \frac{1}{\sqrt{E_s}} \int_{-\frac{T_s}{2}}^{\frac{T_s}{2}} \left[\int_{-\infty}^{\infty} S_{in}(f)\, H(f)\, e^{i2\pi f t}\, df\right] \phi_k(t)\, dt \\ &= \frac{1}{\sqrt{E_s}} \int_{-\infty}^{\infty} S_{in}(f)\, H(f)\, \Phi_k(f)\, df, \end{aligned} \tag{4}$$

where $S_{in}(f)$ is the Fourier transform of the signal at the filter input, $H(f)$ is the transfer function of the filter and

$$\Phi_k(f) = \int_{-\frac{T_s}{2}}^{\frac{T_s}{2}} \phi_k(t)\, e^{i2\pi f t}\, df. \tag{5}$$

It is then straightforward to obtain the signal at the output of the integrator as [17, eq. (1)]

$$x = \int_{-\frac{T_s}{2}}^{\frac{T_s}{2}} |s(t)+n(t)|^2\, dt = \sum_{k=1}^{\infty} \left[\left(\sqrt{E_s}\, s_k + n'_k\right)^2 + n''^2_k\right]. \tag{6}$$

2.2. Proposed BEP evaluation

The probability of erroneous demodulation and BEP in binary PPM with soft decisions is given by

$$P_e^{bppm} = 1 - \int_0^{\infty} \left[\int_0^{x} f_0(u)\, du\right] f_{\mathcal{E}}(x)\, dx, \tag{7}$$

where $f_0(x)$ and $f_{\mathcal{E}}(x)$ denote the probability density functions (pdfs) of the electrical signal at the empty PPM slot and the slot that contains the optical energy, respectively. The integral calculates the probability of correct demodulation, where the measured signal value at the empty slot is less than the corresponding value at the energy containing slot. Following (6), the integrator output x corresponds to the sum of independent χ^2 RVs and, assuming that a finite number of M eigenvalues contribute, the Laplace transform of its pdf $f_{\mathcal{E}}(x)$ is given by [20]

$$F_{\mathcal{E}}(s) = \prod_{k=1}^{M} \frac{\exp\left(-\frac{s\,\mathcal{E}_k}{1+s\,\lambda_k}\right)}{1+s\,\lambda_k}, \tag{8}$$

where $\mathcal{E}_k = s_k^2\, E_s/N_0$. If no signal is present ($\mathcal{E}_k = 0$), the last equation reduces to

$$F_0(s) = \prod_{k=1}^{M} \frac{1}{1 + s\,\lambda_k}\,. \tag{9}$$

After expressing the Laplace transform $F_0(s)$ as the sum

$$F_0(s) = \sum_{k=1}^{M} \frac{c_k}{1 + s\,\lambda_k}\,, \tag{10}$$

with

$$c_k = \left[\prod_{\substack{j=1\\ j\neq k}}^{M} \left(1 - \frac{\lambda_j}{\lambda_k}\right)\right]^{-1}\,, \tag{11}$$

the pdf $f_0(x)$ is calculated as

$$f_0(x) = \sum_{k=1}^{M} \frac{c_k}{\lambda_k} \exp\left(-\frac{x}{\lambda_k}\right)\,. \tag{12}$$

By combining (12) and (7), we arrive at

$$\begin{aligned} P_e^{bppm} &= \int_0^{\infty} \sum_{k=1}^{M} c_k \exp\left(-\frac{x}{\lambda_k}\right) f_{\mathcal{E}}(x)\,dx = \sum_{k=1}^{M} c_k\, F_{\mathcal{E}}\left(\frac{1}{\lambda_k}\right) \\ &= \frac{1}{2} \sum_{k=1}^{M} \exp\left(-\frac{\mathcal{E}_k}{2\,\lambda_k}\right) \prod_{\substack{j=1\\ j\neq k}}^{M} \frac{\exp\left(-\dfrac{\mathcal{E}_j}{\lambda_k + \lambda_j}\right)}{1 - \dfrac{\lambda_j^2}{\lambda_k^2}}\,. \end{aligned} \tag{13}$$

The BEPs for higher PPM orders Q are then approximated as [25]

$$P_e^{qppm} \leq \frac{Q}{2\,(Q-1)} \left[1 - \left(1 - P_e^{bppm}\right)^{Q-1}\right]\,. \tag{14}$$

The advantage of (14) is that it does not require the knowledge of the pdf of (8) that is challenging to calculate analytically.

It should be noted that the proposed model is also valid in systems with weather losses and atmospheric turbulence, although a full treatment of these effects is beyond the scope of this work. In a typical high capacity system, the PPM slot duration amounts to ns [15], and is significantly shorter than the average duration of fades and weather changes. As a result, the channel response is practically flat over the duration of the PPM symbol, and its impact can be introduced by multiplying the symbol energy E_s with the channel response h. The model then correctly predicts that the BEP lowers when weather and fading losses are introduced, due to its exponential dependence on the received energy. Moreover, the model requires a fixed number of terms M and, as we demonstrate in the following sections, is valid for all E_s/N_0. Consequently, the model can be used to assess the performance of the system for any given weather and fading conditions.

2.3. Results and discussion

We first consider an ideal passband optical filter with a flat frequency response over $\left[-B_o/2,\, B_o/2\right]$. The eigenfunctions and the eigenvalues of the filter are calculated from [26] and [27, eq. (30.15.1-2)]

$$\begin{aligned} \phi_k(t) &= \sqrt{\frac{2\,k+1}{T_s}}\, Ps_k^0\left(\frac{2\,t}{T_s}, \gamma^2\right), \qquad |t| \leq \frac{T_s}{2}, \\ \lambda_k &= B_o\,T_s \left[S_k^{0(1)}\left(1\,,\,\gamma\right)\right]^2\,, \end{aligned} \tag{15}$$

where $Ps_k^m(\cdot,\cdot)$ is the angular spheroidal wave function of the first kind [27, eq. (30.4.1)], $S_k^{0(1)}(\cdot,\cdot)$ is the radial spheroidal function of the first kind [27, eq. (30.11.8)] and $\gamma = \pi\, B_o\, T_s/2$. With respect to the signal expansion terms s_k, we first use [27, eq. (30.15.5)] to evaluate the Fourier transform of (5) as

$$\Phi_k(f) = (-1)^k \sqrt{\frac{T_s\,\lambda_k}{B_o}}\, \phi_k\left(-\frac{T_s\,f}{B_o}\right)\,. \tag{16}$$

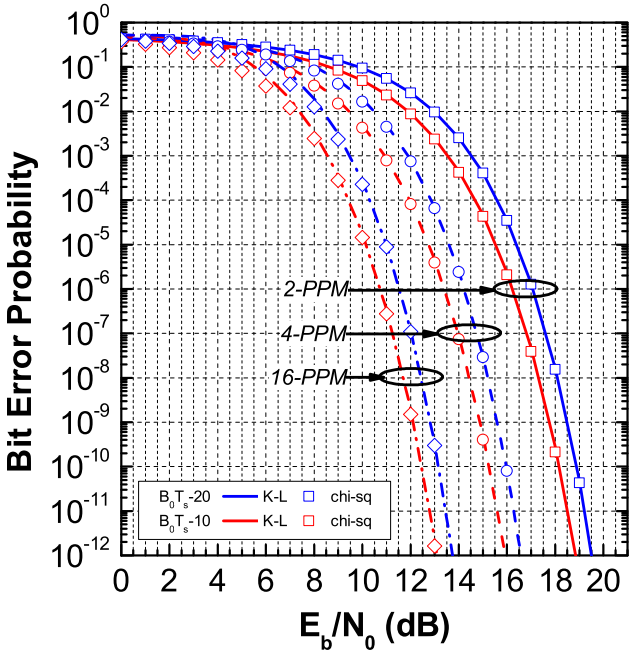

Fig. 2. BEP of the optically pre-amplified receiver with an ideal passband filter for $B_o\,T_s = 10,\, 20$ and $Q = 2,\, 4,\, 16$.

For a square input pulse with amplitude $\sqrt{E_s/T_s}$, (4) evaluates to

$$\begin{aligned} s_k &= (-1)^k \sqrt{\frac{\lambda_k}{B_o}} \int_{-\frac{B_o}{2}}^{\frac{B_o}{2}} \frac{\sin\left(\pi\, f\, T_s\right)}{\pi\, f}\, \phi_k\left(-\frac{T_s\,f}{B_o}\right)\,df \\ &= (-1)^k \sqrt{\frac{2\,k+1}{B_o\,T_s}}\, \lambda_k^{3/2}\, Ps_k^0\left(0, \gamma^2\right)\,, \end{aligned} \tag{17}$$

where we have used [27, eq. (30.15.3)].

Eq. (14) is plotted for the obtained noise and signal expansions in Fig. 2. The summation included the first $M = B_o\,T_s$ eigenvalues, which proved adequate to achieve convergence. The figure also compares the proposed method with the results that are obtained using a χ^2 approximation from previous works [19]. The results are in perfect agreement for $M = 10,\, 20$ and $Q = 2,\, 4,\, 16$, which verifies both the accuracy of the proposed method and the validity of the χ^2 approximation. Wider optical filters can also be modeled and assessed in a similar fashion, however the calculations become more challenging since the most significant eigenvalues are practically equal and the denominator of (13) requires a very high number of significant digits to evaluate without error. In this case, the χ^2 approximation is preferable since it is both accurate and easier to evaluate. It should also be noted that the application of the proposed method in narrower filters may lead to inaccurate results, since the pulse is broadened and energy starts to leak in the neighboring slots. According to our calculations, a time-bandwidth product of $B_o\,T_s \geq 10$ ensures that over 97% of the signal energy is contained within the correct slot.

A second filter with known eigenfunctions and eigenvalues is the Lorentzian response filter, which approximates the response of etalons that are used in pre-amplified PPM systems [28]. The filter has the following frequency response and autocorrelation functions

$$H(f) = \frac{1}{1 + i\,\frac{2\,f}{B_o}} \tag{18}$$

and

$$R_n(\tau) = \frac{\pi\, B_o}{2} \exp\left(-\pi\, B_o\, |\tau|\right)\,, \tag{19}$$

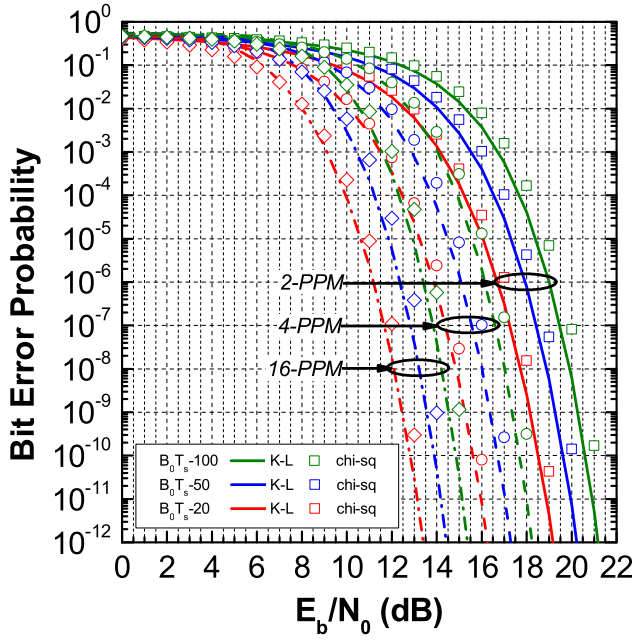

Fig. 3. BEP of the optically pre-amplified receiver with a Lorentzian response filter for $B_o T_s = 20, 50, 100$ and $Q = 2, 4, 16$.

respectively, where $B_o/2$ is the 3 dB bandwidth. The eigenfunctions and eigenvalues are given by [29]

$$\phi_k(t) = \frac{A_k}{\sqrt{T_s}} \left[\frac{\pi\, B_o\, T_s}{2\, z_k} \sin\left(\frac{z_k\,(2\,t + T_s)}{T_s} \right) + \cos\left(\frac{z_k\,(2\,t + T_s)}{T_s} \right) \right], \tag{20}$$

and

$$\lambda_k = \left[1 + \left(\frac{2\, z_k}{\pi\, B_o\, T_s} \right)^2 \right]^{-1}. \tag{21}$$

In the previous equations, A_k are normalization constants and z_k are the solutions to the following equations

$$\frac{\tan(z_k)}{z_k} = -\frac{2}{\pi\, B_o\, T_s}, \tag{22a}$$

and

$$\frac{\cot(z_k)}{z_k} = \frac{2}{\pi\, B_o\, T_s}. \tag{22b}$$

The signal at the filter output equals

$$s(t) = \sqrt{\frac{E_s}{T_s}} \left[1 - \exp\left(-\pi\, B_o \left(t + \frac{T_s}{2} \right) \right) \right] \tag{23}$$

and (4) evaluates to

$$\begin{aligned} s_k &= \frac{1}{\sqrt{T_s}} \int_{-\frac{T_s}{2}}^{\frac{T_s}{2}} \left[1 - e^{-\pi\, B_o \left(t + \frac{T_s}{2} \right)} \right] \phi_k(t)\, dt \\ &= \frac{A_k \sin\left(z_k \right)}{z_k} \left[\frac{\pi\, B_o\, T_s}{2\, z_k} \sin\left(z_k \right) + \cos\left(z_k \right) \right] - \frac{2\, \lambda_k\, A_k}{\pi\, B_o\, T_s}, \end{aligned} \tag{24}$$

where we have utilized (2) at $y = -T_s/2$ to arrive at

$$\int_{-\frac{T_s}{2}}^{\frac{T_s}{2}} e^{-\pi\, B_o \left(t + \frac{T_s}{2} \right)} \phi_k(t)\, dt = \frac{2\, \lambda_k}{\pi\, B_o} \phi_k\left(-\frac{T_s}{2} \right). \tag{25}$$

Eq. (14) is plotted in Fig. 3, after keeping the first $M = 2\, B_o\, T_s$ eigenvalues since the response of the Lorentzian filter is non-zero outside the 3 dB bandwidth. Similarly to the ideal passband filter, we only consider wide optical filters, otherwise the filter output starts to leak into the adjacent slot according to (23). However, the calculations are numerically more stable due to the fact that the eigenvalues are distinct and Lorentzian response filters with wider bandwidths can be assessed. To be consistent with previous works on optically pre-amplified systems that employ a time bandwidth product equal to $B_o\, T_s = 55$ [15], we have considered similar values in our calculations. As expected, the BEP improves when the modulation order is increased and worsens when the optical bandwidth is increased. The results also show that the χ^2 distribution overestimates the BEP by an almost constant factor of less than 0.5 dB, irrespective of the filter bandwidth and modulation order. This observation can also be interpreted as a comparison between the ideal passband and Lorentzian filter responses. In effect, the ideal passband filter introduces a 0.5 dB penalty that can be explained by the fact that more noise is allowed to pass within the signal bandwidth. The Lorentzian response, on the other hand, starts to reject noise at lower frequencies and exhibits better performance, as it has been previously reported for a smaller time bandwidth product and on-off-keying [20].

Regarding the accuracy of the proposed approach for the Lorentzian filter, it is not possible to directly compare the presented BEP results with an existing model. To address this issue and verify the validity of Eq. (14), we performed Monte-Carlo simulations. The simulations involved the generation of $M = 2\, B_o\, T_s$ χ^2 RVs with two degrees of freedom and unequal variances λ_k, as dictated by (6). The χ^2 RVs were then added to generate the received signals at the empty PPM slots. Similarly, the PPM slot that contained the signal energy was generated by adding an equal number of non-central χ^2 RVs with different non-centrality parameters $\mathcal{E}_k$. The slot signals were then compared and the maximum value was considered as the most probable (soft decision decoding), leading to the introduction of errors whenever an empty slot was incorrectly selected. The results of the simulation are shown in Fig. 4, where they are compared with the analytical ones for $Q = 16$ that is expected to introduce the biggest inaccuracy. It can be verified that the discrepancy is very limited at low E_b/N_0 values, while both approaches are in very good agreement with each other at higher E_b/N_0. For comparison purposes, we also present results for the widely used union bound, which is obtained by keeping only the first term of the expression inside the power in Eq. (14). The figure verifies that the proposed model is significantly more accurate than the union-bound at low E_b/N_0, while all three methods (proposed, simulation, union-bound) coincide at high E_b/N_0, thus demonstrating the accuracy of the proposed model.

3. Coded BEP evaluation

For the coded system we consider a conventional forward error correction scheme, as presented in Fig. 1. The LDPC encoder appends parity check bits to the bit stream to construct codewords, which are mapped into PPM symbols by the modulator. At the receiver side, optical noise is added to the PPM symbols and the resulting electrical signal is integrated over the slot duration following Eq. (6). The demodulator calculates the PPM symbol likelihoods from the integrator outputs, and then converts them to bit likelihoods using the methodology that is presented in the following paragraphs. The bit likelihoods are finally fed to the LDPC decoder that attempts to restore the original bit stream.

3.1. LDPC encoder and decoder

Our implementation of error-correction is based on the LDPC codes of the 5G standard [22]. These codes utilize a quasi-cyclic parity-check matrix structure, which is constructed from the permutations of smaller matrices of size $Z_c \times Z_c$ and an appropriate number of block rows and columns. The smaller matrices are either zero matrices or cyclic permutations of the identity matrix and their positions on the block rows and columns are determined using the set index i_{LS}, which contains Z_c. In this work, we only utilize the Base Graph 1 (BG1), which is oriented towards larger data lengths, and we use $Z_c = 384$ to achieve a data length of 8448 bits, since $K_b = 22$ columns are always

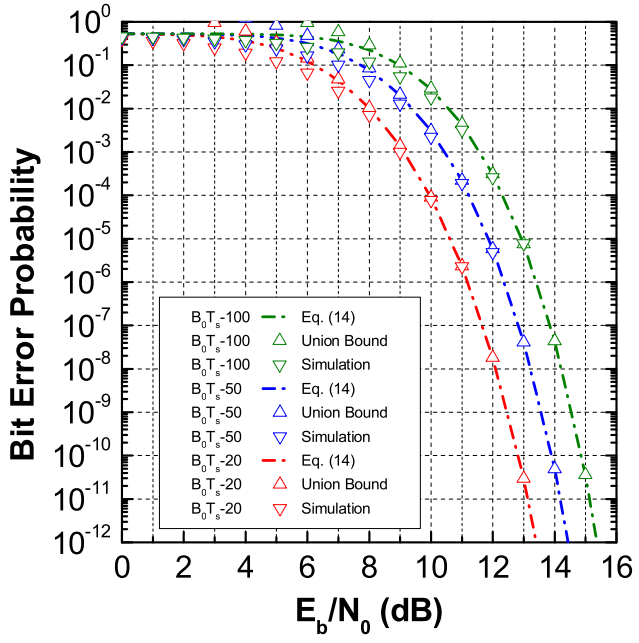

Fig. 4. Comparison between analytical and simulation results for a Lorentzian response filter with $B_o T_s = 20,\ 50,\ 100$ and $Q = 16$.

assigned to the data in BG1. The parity-check matrix for the desired code rate $\mathcal{R}$ is attained by selecting the first $K_b/\mathcal{R}$ block columns and $K_b(1-\mathcal{R})/\mathcal{R}$ block rows of the corresponding base matrix. The parity-check matrix also entails a double-diagonal structure at block columns $(K_b{+}1,\ K_b{+}2,\ \ldots,\ K_b/\mathcal{R})$, which is utilized by the encoder to efficiently calculate the parity bits and construct the codewords.

The codes are capable of correcting short bursts of errors that are introduced by the PPM receiver provided that the parity checks are generated from bits that do not belong to the same symbol. The error burst that is caused by a PPM symbol error, and may lead up to $\log_2(Q)$ consecutive erroneous bits, can then be corrected since each bit belongs to different parity checks and can be corrected independently. Since the parity checks are selected according to the value of Z_c, it is sufficient to require that $Z_c \gg \log_2(Q)$, which is true for practical systems that utilize low PPM orders. In particular, this work considers $Z_c = 384$ and $\log_2(Q) = \{3, 4\}$ and it is therefore expected that the utilized LDPCs will have a high error correction effectiveness [23].

The BEP performance of the LDPC-coded system is evaluated for two popular decoder architectures, the min-sum and the sum–product decoder. The two decoders were implemented using iterative message passing algorithms [30, eq. (22)], which utilize messages $\alpha_{m,n}$ (variable-to-check) and $\beta_{m,n}$ (check-to-variable) to calculate the intrinsic log-likelihood ration (LLR) of each bit γ_n [31]. The sum–product decoder updates messages $\beta_{m,n}$ following

$$\beta_{m,n} = 2\,\tanh^{-1}\left[\prod_{n'\in P_m\setminus\{n\}} \tanh\left(\frac{\alpha_{m,n'}}{2}\right)\right], \tag{26}$$

and the min-sum utilizes the approximation

$$\beta_{m,n} = \prod_{n'\in P_m\setminus\{n\}} \operatorname{sgn}\left(\alpha_{m,n'}\right) \min_{n'\in P_m\setminus\{n\}} |\alpha_{m,n'}|\,, \tag{27}$$

respectively, with $P_m\setminus\{n\}$ denoting the positions of the non-zero entries of the parity-check matrix at row m, except for column n itself. The new values for $\alpha_{m,n}$ and the intrinsic LLR are calculated from

$$\alpha_{m,n} = \gamma_n - \beta_{m,n} \tag{28}$$

and

$$\gamma_n = \rho(b_n) + \sum_{m\in P_n} \beta_{m,n}\,, \tag{29}$$

where P_n contains the positions of the non-zero entries of the parity-check matrix at column n. $\rho(b_n)$ is the extrinsic LLR of each bit and is obtained from the PPM signal values, as it is described in the next paragraph. After each update of the intrinsic LLR values, the decoder translates them into bits and checks if a valid codeword has been found. If the codeword is not valid, the process repeats for a maximum number of 10 iterations in our implementation of both decoders.

3.2. Derivation of the extrinsic LLR

The extrinsic LLR of each bit is calculated from the PPM symbol that contains it. To this end, we first observe that a bit is '0' when the PPM pulse is located in half of the symbol slots, or '1' when the PPM pulse is located in the remaining slots. Two disjoint slot sets are then formed for the ℓth bit: B_ℓ^0 is the set that contains the slots in which the bit is '0' and B_ℓ^1 is the set that contains the slots in which the bit is '1'. The sets are fixed and different for each bit, for example in 4-PPM the slots correspond to the bit combinations $\{s1, s2, s3, s4\} \triangleq \{00, 01, 10, 11\}$ and we find that $B_1^0 = \{s1, s2\}$, $B_1^1 = \{s3, s4\}$, $B_2^0 = \{s1, s3\}$ and $B_2^1 = \{s2, s4\}$. The extrinsic LLR $\rho(b_\ell)$, $\ell = 1, 2, \ldots, \log_2(Q)$ of the ℓth bit is then calculated from [23, eq. (9)-(12)]

$$\rho(b_\ell) = \log\left[\frac{\sum_{i\in B_\ell^0} \Lambda(x_i)}{\sum_{i\in B_\ell^1} \Lambda(x_i)}\right], \tag{30}$$

where x_i, $i = 1, 2, \ldots, Q$ is the received optical signal at the ith PPM slot and $\Lambda(x)$ is the likelihood function

$$\Lambda(x) = \frac{f_{\mathcal{E}}(x)}{f_0(x)}\,. \tag{31}$$

The likelihood function is not known for an arbitrary optical filter shape, since an analytic expression for $f_{\mathcal{E}}(x)$ is not generally available. However, it was previously shown [23] that the individual pdfs can be efficiently approximated by Gaussian functions

$$f_0(x) \approx \frac{1}{\sqrt{2\,\pi\,\sigma_0^2}} \exp\left[-\frac{(x-\mu_0)^2}{2\,\sigma_0^2}\right], \tag{32a}$$

and

$$f_{\mathcal{E}}(x) \approx \frac{1}{\sqrt{2\,\pi\,\sigma_{\mathcal{E}}^2}} \exp\left[-\frac{(x-\mu_{\mathcal{E}})^2}{2\,\sigma_{\mathcal{E}}^2}\right], \tag{32b}$$

using the first two moments of the distributions $f_0(x)$ and $f_{\mathcal{E}}(x)$

$$\begin{aligned} \mu_0 &= \sum_{k=1}^{M} \lambda_k\,, & \sigma_0^2 &= \sum_{k=1}^{M} \lambda_k^2\,, \\ \mu_{\mathcal{E}} &= \sum_{k=1}^{M} \left(\mathcal{E}_k + \lambda_k\right), & \sigma_{\mathcal{E}}^2 &= \sum_{k=1}^{M} \left(2\,\mathcal{E}_k\,\lambda_k + \lambda_k^2\right). \end{aligned} \tag{33}$$

This leads to a similar Gaussian approximation for the likelihood function, and after some algebra the extrinsic LLR of each bit is calculated following

$$\begin{aligned} \rho(b_\ell) &\approx \log\left[\max_{i\in B_\ell^0} \Lambda(x_i)\right] - \log\left[\max_{i\in B_\ell^1} \Lambda(x_i)\right] \\ &\approx \frac{\sigma_{\mathcal{E}}^2 - \sigma_0^2}{2\,\sigma_{\mathcal{E}}^2\,\sigma_0^2}\left(\max_{i\in B_\ell^0} x_i - \max_{i\in B_\ell^1} x_i\right) \\ &\quad \times \left(\max_{i\in B_\ell^0} x_i + \max_{i\in B_\ell^1} x_i - 2\,\frac{\mu_0\,\sigma_{\mathcal{E}}^2 - \mu_{\mathcal{E}}\,\sigma_0^2}{\sigma_{\mathcal{E}}^2 - \sigma_0^2}\right). \end{aligned} \tag{34}$$

In the last expression, we have only kept the contribution of the maximum signal in each of the two sets, assuming that the rest of the signals do not contribute significantly to the sum of (30) due to the rapidly increasing likelihood function [32, eq. (8)]. A further

simplification can be made for the min-sum decoder by ignoring the constant terms to arrive at

$$\rho(b_\ell) \approx \left(\max_{i\in B_\ell^0} x_i\right)^2 - \left(\max_{i\in B_\ell^1} x_i\right)^2 . \tag{35}$$

3.3. Code rate optimization

The coded BEP of the two decoders was evaluated with Monte-Carlo simulations for a Lorentzian response filter, while the ideal passband filter has been studied in a previous work [23]. Random streams that contained 8448 bits were encoded using the double-diagonal structure of the LDPC parity check matrix, and the generated codewords were partitioned into PPM symbols. In each symbol, the empty slot signals were generated by summing $M = 2\,B_o T_s$ central χ^2 RVs with two degrees of freedom and unequal variances λ_k, as it has been detailed in the analysis of the uncoded system. The signal at the slot that contained the symbol energy was generated in a similar manner by summing an equal number of non-central χ^2 RVs with different non-centrality parameters $\mathcal{R}\,\mathcal{E}_k$, where $\mathcal{R}$ denotes the code-rate. The slot signals x_i were then utilized to approximate the extrinsic LLRs and decode the received bit sequences via message-passing. The simulations were performed for a confidence level of 99% for the BEP and 90% for the Frame Error Probability (FEP), using the confidence interval upper and lower limits given by [33, eq. (11.2.11)]. The simulations repeated until the width of the confidence intervals was less than 10% of the measured BEP and FEP, resulting in the accurate estimation of their actual values.

Fig. 5 presents the simulation results for the min-sum decoder and code rates equal to $\mathcal{R} = 1/2,\ 2/3,\ 11/13$. The results show that the code rate is an important design parameter and the optimal performance is expected for code rates between 2/3 and 11/13. The unanimously best selection for the code rates that are presented in the figure is 11/13. The 2/3 rate performs equally well for $Q = 4$ and $B_o T_s = 20$, but it introduces a small energy penalty of up to 0.1 dB for wider filters. Similar observations can be made for $Q = 16$, where the energy penalty of the 2/3 rate is somewhat increased to over 0.2 dB. Finally, the 1/2 rate introduces a more significant penalty that increases with the filter bandwidth and ranges between 0.2–0.4 dB for $Q = 4$, and 0.5–0.7 dB for $Q = 16$. The sum–product decoder results are presented in Fig. 6. Again, the optimal performance is expected for code rates between 2/3 and 11/13, but the best selection depends on the modulation order. The 2/3 rate is the best selection for $Q = 4$ and the 11/13 rate is the best selection for $Q = 16$, with their penalty difference being less than 0.2 dB in all cases. The 1/2 rate performs worse than the other two in all cases, and introduces a penalty of up to 0.6 dB for $Q = 16$ and $B_o T_s = 100$.

3.4. Performance comparison

The optimization of the code rate enables the assessment of the effectiveness of the LDPC codes in the pre-amplified system. Using the optimal code rates and the results of Figs. 3 and 6, it can be verified that the coded system provides a very significant performance improvement that depends on the target BEP. If for example a target BEP of 10^{-5} is considered, then the maximum energy gain of the coded system can exceed 3 dB for $Q = 4$ with a narrow filter. It can also be observed that the increase in the modulation order from $Q = 4$ to $Q = 16$ reduces the effectiveness of the LDPC error correction by approximately 0.5 dB. Similarly, wider optical filters also reduce the effectiveness and approximately 0.2 dB are lost when the optical filter bandwidth doubles. Table 1 summarizes the effectiveness of the LDPC error correction for both modulation orders and all time bandwidth products.

By comparing Figs. 5 and 6, it can also be seen that the min-sum decoder does not introduce a significant performance degradation

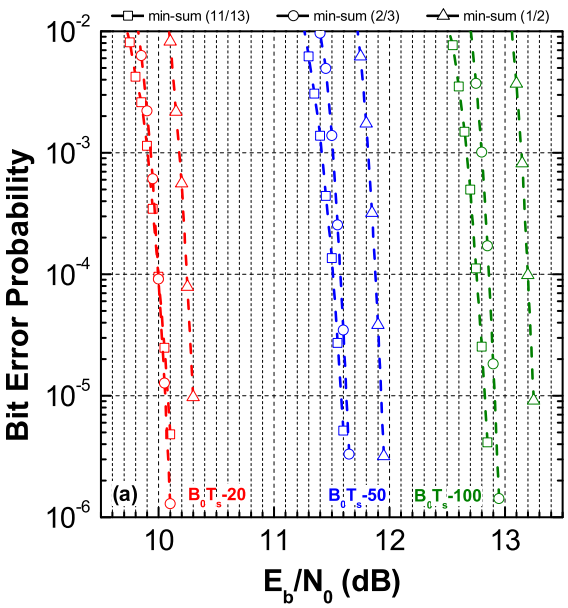

(a) The PPM modulation order is $Q = 4$.

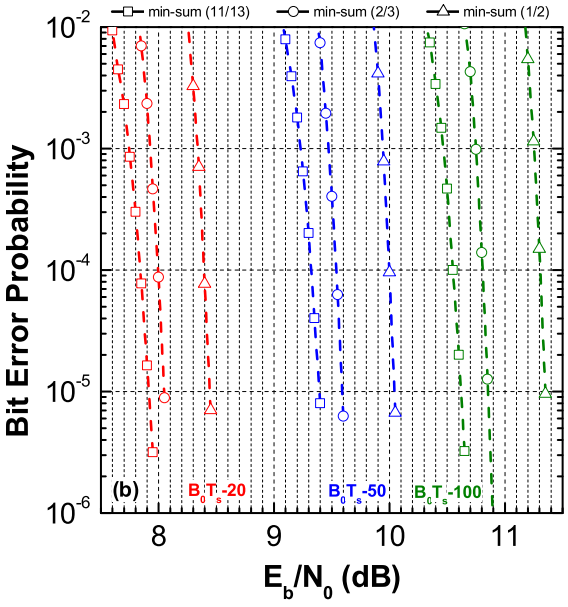

(b) The PPM modulation order is $Q = 16$.

Fig. 5. BEP of the min-sum decoder for a Lorentzian response filter with $B_o T_s$ = 20, 50, 100.

Table 1
E_b/N_0 that is required to attain a target BEP of 10^{-5}.

	$Q = 4$		
	$B_o T_s = 20$	$B_o T_s = 50$	$B_o T_s = 100$
Uncoded	13.2 dB	14.5 dB	15.6 dB
Coded	9.9 dB	11.5 dB	12.8 dB
Gain	3.3 dB	3.0 dB	2.8 dB
	$Q = 16$		
	$B_o T_s = 20$	$B_o T_s = 50$	$B_o T_s = 100$
Uncoded	10.6 dB	11.9 dB	12.9 dB
Coded	7.9 dB	9.4 dB	10.6 dB
Gain	2.7 dB	2.5 dB	2.3 dB

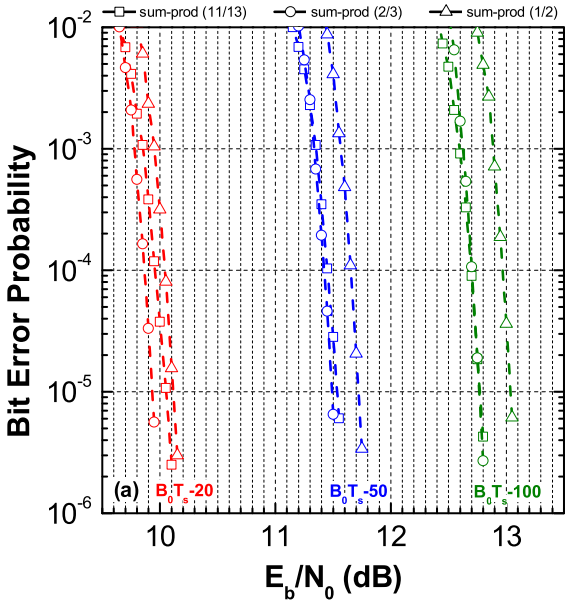

(a) The PPM modulation order is $Q = 4$.

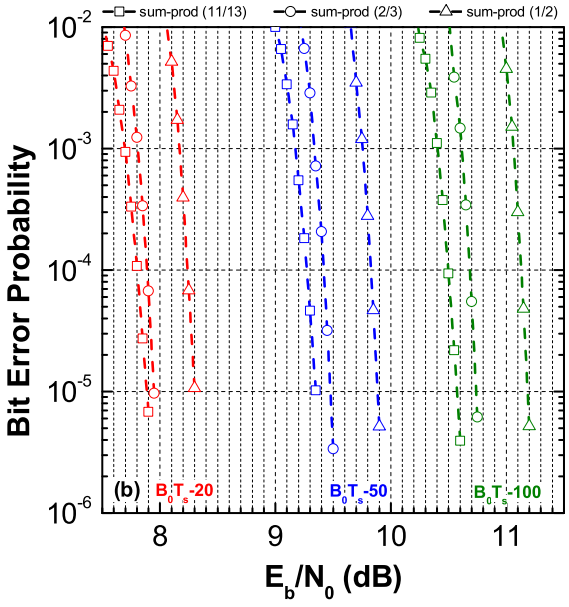

(b) The PPM modulation order is $Q = 16$.

Fig. 6. BEP of the sum–product decoder for a Lorentzian response filter with $B_o T_s = 20, 50, 100$.

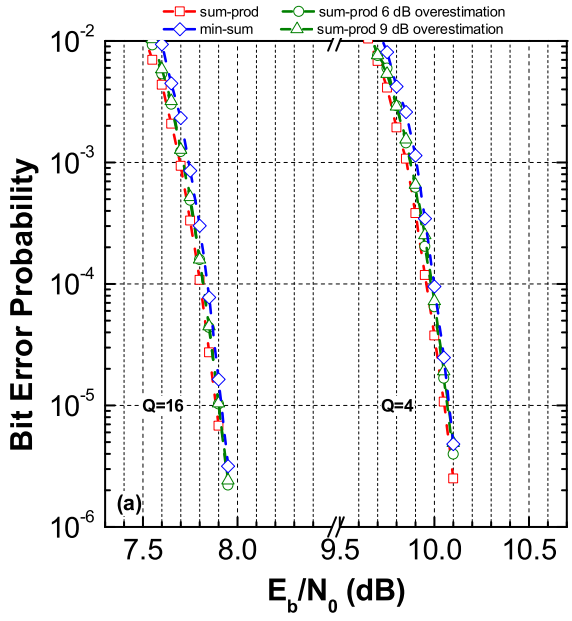

(a) Overestimation of E_b/N_0.

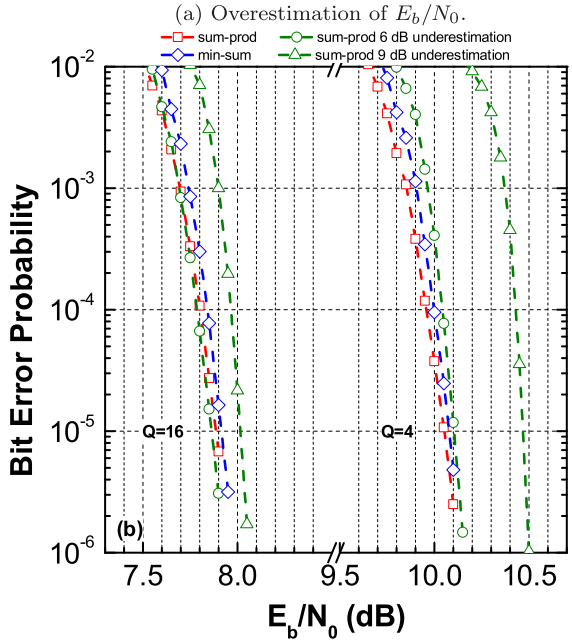

(b) Undestimation of E_b/N_0.

Fig. 7. Impact of imperfect E_b/N_0 knowledge on the BEP performance. The code rate is equal to $\mathcal{R} = 11/13$ and the time-bandwidth product is $B_o T_s = 20$.

despite its simplified LLR expression, provided that the best possible code rate is used. The maximum difference between the two decoders is slightly over 0.1 dB and is observed for $Q = 4$ and $B_o T_s = 20$. This gain may only be achieved provided that the sum–product decoder has knowledge or an accurate estimation of the parameters of (33). Following previous works [34], imperfect knowledge of the parameters that leads to the overestimation of E_b/N_0 degrades the performance of the sum–product decoder, which becomes identical to that of the min-sum one. However, the underestimation of E_b/N_0 introduces a more significant degradation, and the sum–product BEP reverts to that of the uncoded system.

Both cases are quantified in Fig. 7, where E_b/N_0 is overestimated and underestimated by 6 and 9 dB in a system with $B_o T_s = 20$ and $\mathcal{R} = 11/13$. It can be verified that the overestimation results in a penalty of at most 0.1 dB and therefore has a limited effect. In contrast, the underestimation gradually renders the sum–product decoder BEP worse than the min-sum one. The system with $Q = 4$ is more sensitive to the imperfect knowledge and an underestimation of approximately 6 dB is required before the sum–product decoder begins to underperform. When the modulation order is increased to $Q = 16$, the allowable underestimation increases and must attain a value between 6–9 dB before the sum–product decoder performance is worse than the min-sum one. This analysis shows that perfect knowledge is not required, but even partial knowledge may not justify the cost and complexity of the estimation subsystem given the limited performance gain that is expected. As a result, the min-sum decoder may prove particularly appealing in practical systems, since it does not require the knowledge or estimation of any of the parameters. Moreover, both the present results

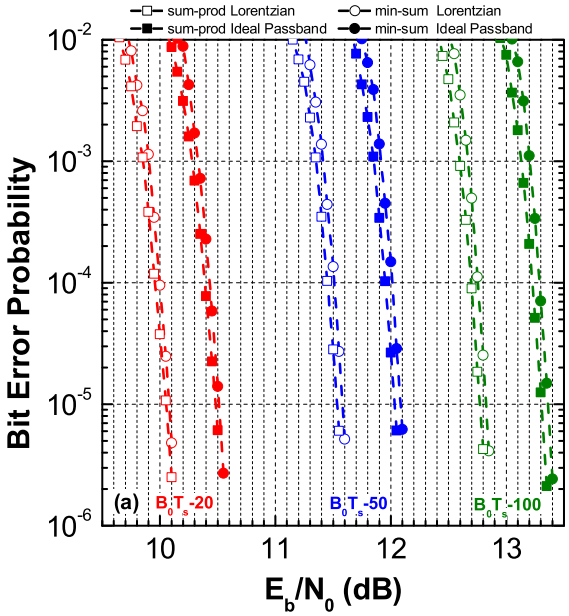

(a) The PPM modulation order is $Q = 4$.

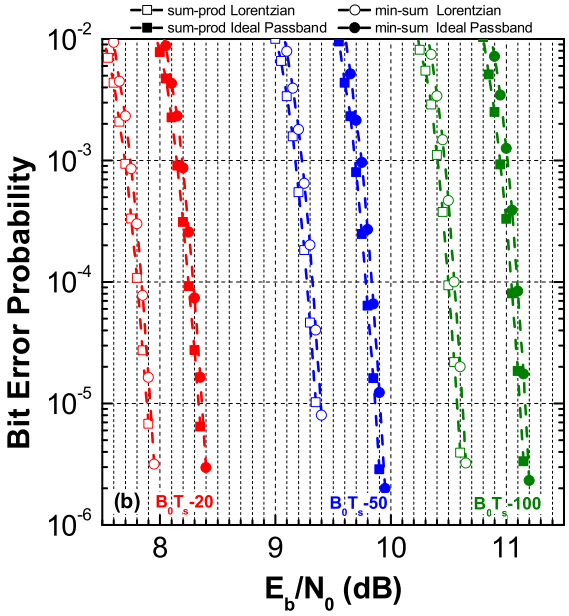

(b) The PPM modulation order is $Q = 16$.

Fig. 8. BEP comparison of coded systems with Lorentzian and ideal passband filters. The code rate is equal to $\mathcal{R} = 11/13$.

and the results of a previous work on ideal passband filters [23] verify the validity of (35). It is then reasonable to conjecture that the min-sum decoder can be utilized without alteration in all systems irrespective of their optical filter response, as long as their time-bandwidth product is high. This is typically a requirement in practical systems, where the time bandwidth product exceeds $B_o T_s = 50$ [15].

Finally, Fig. 8 provides a comparative analysis between coded systems with Lorentzian and ideal passband filters. The code rate equals $\mathcal{R} = 11/13$ so as to perform a fair comparison between optimized systems [23]. It can be verified that the ideal passband filter introduces a penalty of 0.5 dB compared to a Lorentzian filter with the same time-bandwidth product. This holds true for all time-bandwidth products and both modulation orders, in agreement with what has been observed for the uncoded system.

4. Conclusion

We presented novel analytical expressions for the BEP of optically pre-amplified PPM receivers with arbitrary optical filter response. The analytical expressions utilized the K-L expansion of the signal and noise, and calculate the BEP via the Laplace transform of the signal and noise distributions. The proposed model was applied to analytically evaluate the BEP of the practically used ideal passband and Lorentzian response filters with high optical bandwidths. The results verified that the χ^2 approximation provides accurate results for the ideal passband filter, while it overestimates the BEP for the Lorentzian response filter by 0.5 dB. The method is also applicable for any type of optical filter and can be used to explore the system performance with different filters in future works. Moreover, the method is valid for all signal energy levels and can be applied to accurately assesses the impact of adverse weather and turbulence conditions in separate studies.

We also simulated the performance of the system when LDPC codes are introduced for error-correction. To this end, we first proposed an approximate expression for the bit likelihoods that are required for decoding. We then demonstrated via simulations that the introduction of LDPC error correction imparts a significant energy gain that depends on the modulation order and the filter bandwidth. The maximum expected gain of 3.3 dB was observed for 4-PPM and a time-bandwidth product $B_o T_s = 20$, while the utilization of 16-PPM reduces the gain by approximately 0.5 dB. Additionally, wider optical filters introduce a further loss and approximately 0.2 dB are lost each time the optical bandwidth doubles. The simulations also revealed that the sum–product and min-sum decoders perform within approximately 0.1 dB difference for the most efficient code rates, which range between 2/3 and 11/13. However, the sum–product decoder is sensitive to the imperfect knowledge of the system parameters. Our simulations verify that the overestimation of the E_b/N_0 results in an identical performance between the two decoders, while its underestimation leads to a more severe performance degradation and the sum–product decoder may perform worse than the min-sum one. The exact underestimation level depends on the modulation order, with 4-PPM being more sensitive, however up to 6 dB can be tolerated without a significant performance loss. Finally, a comparison between the coded performance of Lorentzian and ideal passband filters yields the same 0.5 dB improvement of the former that was observed in the uncoded systems.

CRediT authorship contribution statement

Konstantinos Yiannopoulos: Writing – review & editing, Writing – original draft, Methodology. **Nikos C. Sagias:** Writing – review & editing, Writing – original draft, Methodology. **Ioannis Moscholios:** Writing – review & editing, Writing – original draft, Methodology, Conceptualization.

Declaration of competing interest

The authors declare that they have no known competing financial interests or personal relationships that could have appeared to influence the work reported in this paper.

Data availability

Data will be made available on request.

Acknowledgment

A preliminary version of this work has been published in PACET 2024 Conference Proceedings [35].

References

[1] Razavi M, Shapiro JH. Wireless optical communications via diversity reception and optical preamplification. IEEE Trans Wireless Commun 2005;4(3):975–83. http://dx.doi.org/10.1109/TWC.2005.847102.

[2] Karimi M, Nasiri-Kenari M. Free space optical communications via optical amplify-and-forward relaying. J Lightwave Technol 2011;29(2):242–8. http://dx.doi.org/10.1109/JLT.2010.2102003.

[3] Kashani MA, Rad MM, Safari M, Uysal M. All-optical amplify-and-forward relaying system for atmospheric channels. IEEE Commun Lett 2012;16(10):1684–7. http://dx.doi.org/10.1109/LCOMM.2012.082012.121066.

[4] Aladeloba AO, Phillips AJ, Woolfson MS. Performance evaluation of optically preamplified digital pulse position modulation turbulent free-space optical communication systems. IET Optoelectron 2012;6(1):66–74. http://dx.doi.org/10.1049/iet-opt.2011.0029.

[5] Zhao W, Han Y, Yi X. Error performance analysis for FSO systems with diversity reception and optical preamplification over gamma–gamma atmospheric turbulence channels. J Modern Opt 2013;60(13):1060–8. http://dx.doi.org/10.1080/09500340.2013.831137.

[6] Landolsi T, Elrefaie AF. Performance evaluation of optically preamplified PPM systems with dual-polarized ASE noise and finite extinction ratios. IEEE Trans Commun 2014;62(10):3644–51. http://dx.doi.org/10.1109/TCOMM.2014.2359214.

[7] Saxena P, Mathur A, Bhatnagar MR. BER performance of an optically pre-amplified FSO system under turbulence and pointing errors with ASE noise. J Opt Commun Netw 2017;9(6):498–510. http://dx.doi.org/10.1364/JOCN.9.000498.

[8] Elsayed EE, Yousif BB. Performance enhancement of M-ary pulse-position modulation for a wavelength division multiplexing free-space optical systems impaired by interchannel crosstalk, pointing error, and ASE noise. Opt Commun 2020;475:126219. http://dx.doi.org/10.1016/j.optcom.2020.126219.

[9] Sharma K, Grewal SK. Performance assessment of hybrid PPM–BPSK–SIM based FSO communication system using time and wavelength diversity under variant atmospheric turbulence. Opt Quantum Electron 2020;52(10):430. http://dx.doi.org/10.1007/s11082-020-02547-7.

[10] Hayal MR, Yousif BB, Azim MA. Performance enhancement of DWDM-FSO optical fiber communication systems based on hybrid modulation techniques under atmospheric turbulence channel. Photonics 2021;8(11). http://dx.doi.org/10.3390/photonics8110464.

[11] Nouri H, Sait SM, Uysal M. Adaptive modulation for FSO IM/DD systems with multiple transmitters and receivers. IEEE Commun Lett 2023;27(2):586–90. http://dx.doi.org/10.1109/LCOMM.2022.3222992.

[12] Zhang X, Liu W, Huang N, Xu Z. Orthogonal waveform-based backscattering interference suppression technique for underwater optical wireless communication. J Opt Soc Amer A 2024;41(7):1372–80. http://dx.doi.org/10.1364/JOSAA.527301.

[13] Caplan DO, Robinson BS, Murphy RJ, Stevens ML. Demonstration of 2.5-gslot/s optically-preamplified M-PPM with 4 photons/bit receiver sensitivity. In: Optical fiber communication conference and exposition and the national fiber optic engineers conference. Optical Society of America; 2005, p. PDP32. http://dx.doi.org/10.1109/OFC.2005.193210.

[14] Boroson DM, Scozzafava JJ, Murphy DV, Robinson BS, Lincoln MIT. The lunar laser communications demonstration (LLCD). In: 2009 third IEEE international conference on space mission challenges for information technology. 2009, p. 23–8. http://dx.doi.org/10.1109/SMC-IT.2009.57.

[15] Stevens ML, Boroson DM. A simple delay-line 4-PPM demodulator with near-optimum performance. Opt Express 2012;20(5):5270–80. http://dx.doi.org/10.1364/OE.20.005270.

[16] Khatri FI, Robinson BS, Semprucci MD, Boroson DM. Lunar laser communication demonstration operations architecture. Acta Astronaut 2015;111:77–83. http://dx.doi.org/10.1016/j.actaastro.2015.01.023.

[17] Humblet PA, Azizoglu M. On the bit error rate of lightwave systems with optical amplifiers. J Lightwave Technol 1991;9(11):1576–82. http://dx.doi.org/10.1109/50.97649.

[18] Ulmer TG, Henion SR, Walther FG. Power penalty from amplified spontaneous emission in spatial diversity links for fade mitigation. IEEE Photonics Technol Lett 2009;21(3):170–2. http://dx.doi.org/10.1109/LPT.2008.2009318.

[19] Yiannopoulos K, Sagias NC, Boucouvalas AC. Average error probability of an optically pre-amplified pulse-position modulation multichannel receiver under malaga-M fading. Appl Sci 2020;10(3). http://dx.doi.org/10.3390/app10031141.

[20] Alić N, Papen GC, Saperstein RE, Milstein LB, Fainman Y. Signal statistics and maximum likelihood sequence estimation in intensity modulated fiber optic links containing a single optical preamplifier. Opt Express 2005;13(12):4568–79. http://dx.doi.org/10.1364/OPEX.13.004568.

[21] McDonough RN, Whalen AD. Detection of signals in noise. 2nd ed.. Academic Press; 1995.

[22] Richardson T, Kudekar S. Design of low-density parity check codes for 5G new radio. IEEE Commun Mag 2018;56(3):28–34. http://dx.doi.org/10.1109/MCOM.2018.1700839.

[23] Yiannopoulos K, Sagias NC. BEP evaluation of 5G LDPC codes in a pre-amplified optical PPM receiver. Phys Commun 2024;62:102255. http://dx.doi.org/10.1016/j.phycom.2023.102255.

[24] Hamkins J. Performance of binary turbo-coded 256-ary pulse-position modulation. In: TMO progress report 42-13. 1999, p. 1–15.

[25] Hughes LW. A simple upper bound on the error probability for orthogonal signals in white noise. IEEE Trans Commun 1992;40(4):670. http://dx.doi.org/10.1109/26.141419.

[26] Slepian D, Sonnenblick E. Eigenvalues associated with prolate spheroidal wave functions of zero order. Bell Syst Tech J 1965;44(8):1745–59. http://dx.doi.org/10.1002/j.1538-7305.1965.tb04200.x.

[27] https://dlmf.nist.gov/.

[28] Hamid S, Elrefaie A, Hassan M, Landolsi T. Performance evaluation for 64-ary and 16-ary optically pre-amplified PPM systems with Fabry–Pérot filters and finite extinction ratio. In: 2013 1st international conference on communications, signal processing, and their applications. ICCSPA, 2013, p. 1–4. http://dx.doi.org/10.1109/ICCSPA.2013.6487302.

[29] Youla D. The solution of a homogeneous Wiener-hopf integral equation occurring in the expansion of second-order stationary random functions. IRE Trans Inf Theory 1957;3(3):187–93. http://dx.doi.org/10.1109/TIT.1957.1057414.

[30] Kschischang F, Frey B, Loeliger H-A. Factor graphs and the sum-product algorithm. IEEE Trans Inform Theory 2001;47(2):498–519. http://dx.doi.org/10.1109/18.910572.

[31] Savin V. Self-corrected min-sum decoding of LDPC codes. In: 2008 IEEE international symposium on information theory. 2008, p. 146–50. http://dx.doi.org/10.1109/ISIT.2008.4594965.

[32] Robertson P, Villebrun E, Hoeher P. A comparison of optimal and sub-optimal MAP decoding algorithms operating in the log domain. In: Proceedings IEEE international conference on communications ICC '95. Vol. 2, 1995, p. 1009–13. http://dx.doi.org/10.1109/ICC.1995.524253, vol.2.

[33] Jeruchim MC, Balaban P, Shanmugan KS. Simulation of communication systems. 2nd ed.. Springer; 2000, http://dx.doi.org/10.1007/b117713.

[34] Saeedi H, Banihashemi AH. Performance of belief propagation for decoding LDPC codes in the presence of channel estimation error. IEEE Trans Commun 2007;55(1):83–9. http://dx.doi.org/10.1109/TCOMM.2006.887488.

[35] Yiannopoulos K, Sagias NC, Moscholios I. BEP of an optically pre-amplified PPM receiver with arbitrary optical filter response. In: 2024 panhellenic conference on electronics and telecommunications. PACET, 2024, p. 1–4. http://dx.doi.org/10.1109/PACET60398.2024.10497052.